Otology & Neurotology
35:1780–1784 © 2014, Otology & Neurotology, Inc.

Neural Substrates of Conversion Deafness in a Cochlear Implant Patient: A Molecular Imaging Study Using $H_2{}^{15}O$-PET

*Jae-Jin Song, †Griet Mertens, ‡Steven Deleye, ‡Steven Staelens, ‡Sarah Ceyssens, †Annick Gilles, †Marc de Bodt, §‖Sven Vanneste, ¶#Dirk De Ridder, **Euitae Kim, *Sung Joon Park, and †‖Paul Van de Heyning

**Department of Otorhinolaryngology–Head and Neck Surgery, Seoul National University Bundang Hospital, Seongnam, Korea; †Department of Otorhinolaryngology and Head and Neck Surgery, University Hospital Antwerp, Edegem, Belgium; ‡Molecular Imaging Center, University of Antwerp, Edegem, Belgium; §School of Behavioral and Brain Sciences, The University of Texas at Dallas, Dallas, Texas, U.S.A.; ‖Department of Translational Neuroscience, Faculty of Medicine, University of Antwerp, Edegem, Belgium; ¶Department of Surgical Sciences, Section of Neurosurgery, Dunedin School of Medicine, University of Otago, Dunedin, New Zealand; #BRAI^{2}N, Sint Augustinus Hospital, Antwerp, Belgium; and **Department of Neuropsychiatry, Seoul National University Bundang Hospital, Seongnam, Korea*

Objective: Conversion deafness is characterized by sudden hearing loss without any identifiable cause. In the current study, we investigated presumed conversion deafness in a cochlear implant user using $H_2{}^{15}O$–positron emission tomography (PET) scan with speech and noise stimuli in conjunction with audiologic tests such as impedance test and auditory response telemetry. Also, by performing a follow-up PET scan after recovery and comparing prerecovery and postrecovery scans, we attempted to find possible neural substrates of conversion deafness.

Patient: A 51-year-old man with conversion deafness after 4 years of successful cochlear implant use.

Intervention: Supportive psychotherapy.

Main Outcome Measures: Prerecovery and postrecovery $H_2{}^{15}O$-PET scans

Results: The prerecovery $H_2{}^{15}O$-PET scan revealed auditory cortex activation by sound stimuli, which verified normal stimulation of the central auditory pathway. Notably, compared with the prerecovery state, the postrecovery state showed relative activation in the right auditory cortex both under the speech and noise stimulus conditions. Moreover, the bilateral prefrontal and parietal areas were activated more in the postrecovery state than in the prerecovery state. In other words, relative deactivation of the prefronto-parieto-temporal network, a network responsible for conscious sensory perception, or relative dysfunction of top-down and bottom-up attention shifting mediated by the ventral and the dorsal parietal cortices, may have resulted in conversion deafness in the patient.

Conclusion: Relative deactivation of the prefronto-parieto-temporal network or dysfunction in the ventral and the dorsal parietal cortices may be related to the development of conversion deafness.

Key Words: Cochlear implants—Conversion disorder—Positron emission tomography.

Otol Neurotol **35:**1780–1784, 2014.

A conversion disorder manifests as motor or sensory neurologic symptoms but cannot be fully explained neurophysiologically (1). Of them, *conversion deafness* is characterized by sudden hearing loss without any identifiable cause (2). There have been few reports on conversion deafness in patients with a cochlear implant (CI) (3). When a CI recipient presents with symptoms of device failure but shows normal device integrity, it is classified as *performance decrement and adverse reactions*, and an explantation-reimplantation is recommended by the international consensus group (4). Indeed, a misdiagnosis with

Address correspondence and reprint requests to Jae-Jin Song, M.D., Ph.D., Department of Otorhinolaryngology–Head and Neck Surgery, Seoul National University Bundang Hospital, 166 Gumi-Ro, Bundang-Gu, Seongnam, 463-707, Korea; E-mail: jjsong96@gmail.com; jjsong96@snubh.org

This work was supported by Research Foundation Flanders (FWO), the Tinnitus Research Initiative, The Neurological Foundation of New Zealand, TOP project University Antwerp, the Korean Science and Engineering Foundation (KOSEF) grant funded by the Korean government (no. 2006-2005090), and the Basic Science Research Program through the National Research Foundation of Korea (NRF) funded by the Ministry of Education, Science and Technology (2012R1A6A3A03038293).

The authors disclose no conflicts of interest.

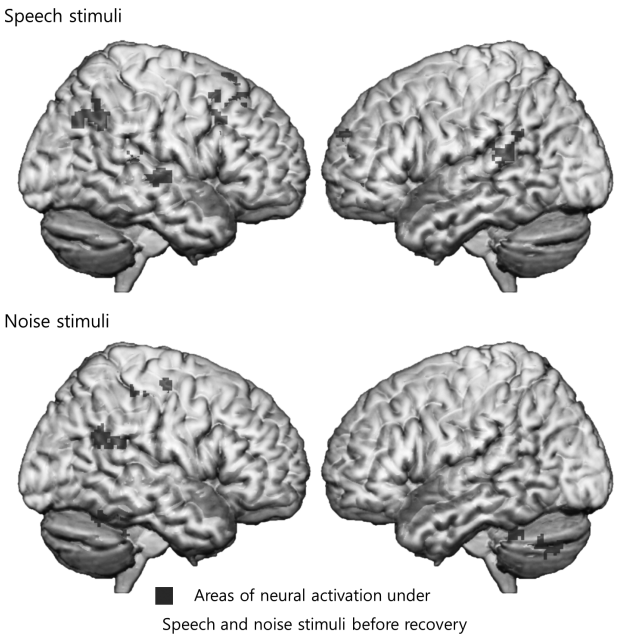

FIG. 1. Main activation effects for the two active stimulus conditions during the symptomatic period (uncorrected $p < 0.05$, $k = 100$ voxels, $T = 3.30$).

device failure in a CI patient with conversion deafness has led to revisions without any clinical benefit (3).

Henceforth, we are reporting on our experience in a CI patient with conversion deafness. The patient underwent $H_2{}^{15}O$–positron emission tomography (PET) scans during the symptomatic period of conversion deafness and after recovery, and thus we were able to investigate the neural substrates of conversion deafness.

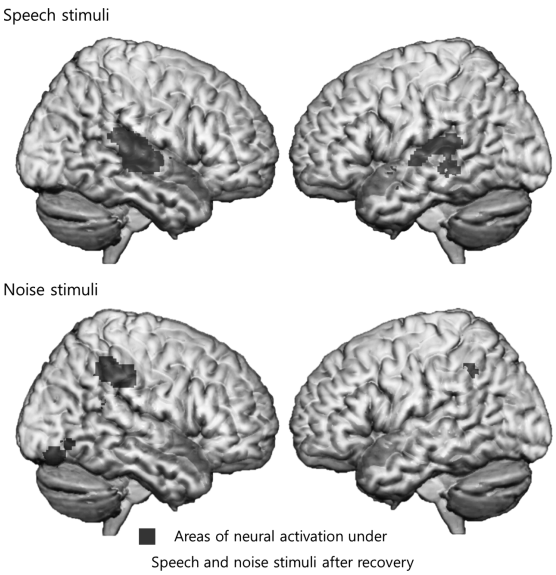

FIG. 2. Main activation effects for the two active stimulus conditions after recovery (uncorrected $p < 0.05$, $k = 100$ voxels, $T = 3.30$).

MATERIALS AND METHODS

Participant

A 51-year-old right-handed man with postlingual deafness underwent left CI (Med-El PULSAR CI100 with FLEXsoft electrode) in 2007. The free-field Fletcher Index (average threshold for 0.5, 1, and 2 kHz) (5,6) in April 2010 indicated a warble tone threshold of 45 dB HL.

In November 2011, the patient reported that he could not hear any sound via the implant. On audiologic evaluation, he did not respond to warble tones or speech tests. However, in-house impedance and speech processor tests as well as device investigation tests by the manufacturer failed to reveal device malfunction. Moreover, reliable spiral ganglion evoked potentials were measured by auditory response telemetry. Further detailed history taking and medical record review revealed a recent succession of stressful life events.

Given the recent history of stressful life events and normal device integrity, the patient was planned to undergo a $H_2{}^{15}O$-PET scan with auditory stimuli, under the impression of conversion deafness. To observe cerebral cortical responses to different auditory stimuli, we planned to adopt speech and white noise stimuli. After the first PET scan, the patient was diagnosed with conversion deafness according to the *Diagnostic and Statistical Manual of Mental Disorders, Fourth Edition* criteria (7). The patient underwent several sessions of counseling and a sham transcranial direct current stimulation (8) and eventually recovered 3 months after onset of the symptom. Postrecovery audiologic examination revealed the same prerecovery hearing thresholds.

PET Study

We adopted three different stimulus conditions: speech stimulus with a Dutch read story, noise stimulus with white nose, and a null condition. We instructed the patient on the three different stimulus conditions that were mixed in a random order. In the auditory stimuli conditions, speech or white noise stimuli are presented directly to the external audio processor via an audio cable. For each condition, three scans were obtained.

The PET/computed tomography scans were acquired using a Siemens Biograph 64 TOF MI PET/computed tomography

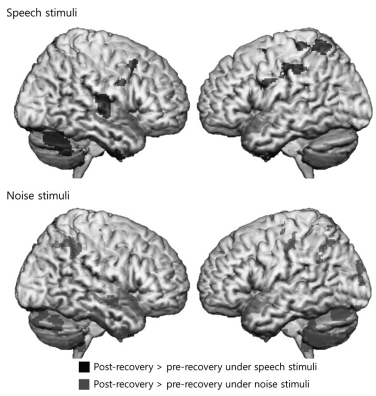

FIG. 3. In the upper panel, brain regions where activity is higher after recovery than before recovery under the speech stimulus condition are displayed (uncorrected $p < 0.005$, $k = 100$ voxels, $T = 4.30$). In the lower panel, brain regions where activity is higher after recovery than before recovery under the speech stimulus condition are displayed (uncorrected $p < 0.005$, $k = 100$ voxels, $T = 4.30$).

TABLE 1. *Areas of neural activation under speech and noise stimuli before and after recovery (uncorrected $p < 0.05$, $k = 100$ voxels, $T = 3.30$)*

Region	Hemisphere	BA	Peak MNI coordinates (x, y, z)			Cluster size (k)	T value
Before recovery							
Areas of neural activation under speech stimuli							
Superior temporal gyrus	R	41	56	−18	4	162	7.5
Superior temporal gyrus	R	41	46	−36	12	112	6.1
Precuneus	R	7	2	−54	44	116	5.9
Middle frontal gyrus	R	9	32	22	32	149	5.3
Superior frontal gyrus	R	8	24	32	46	167	4.9
Inferior parietal lobule	R	40	44	−58	36	219	4.6
Superior temporal gyrus	L	22	−60	−42	18	103	7.1
Middle frontal gyrus	L	11	−28	46	−12	187	6.4
Superior frontal gyrus	L	10	−18	52	18	173	6.1
Anterior cingulate cortex		32	0	38	−6	101	6.7
Areas of neural activation under noise stimuli							
Precentral gyrus	R	4	36	−14	58	162	6.6
Cerebellar tonsil	R		30	−44	−38	103	5.9
Angular gyrus	R	39	58	−56	24	187	4.1
Cerebellar semilunar lobule	L		−44	−74	−40	101	5.4
After recovery							
Areas of neural activation under speech stimuli							
Superior temporal gyrus	R	22	64	−16	2	2386	12.1
	R	41	48	−28	4	i.above	7.2
	R	42	70	−30	18	i.above	4.0
Superior temporal gyrus	L	22	−68	8	−2	272	4.7
Middle temporal gyrus	L	21	−66	0	−14	i.above	3.4
Superior temporal gyrus	L	22	−68	−38	14	664	4.4
	L	22	−60	−12	0	i.above	4.3
Areas of neural activation under noise stimuli							
Inferior parietal lobule	R	40	54	−30	38	587	5.5
Cerebellar declive	R		42	−78	−16	237	4.7
Middle occipital gyrus	R	19	50	−70	−8	i.above	2.5
Insula	R	13	44	−42	20	115	4.1
Inferior parietal lobule	L	40	−40	−50	44	108	4.4
Supramarginal gyrus	L	40	−36	−48	32	i.above	2.8

BA indicates Brodmann area; MNI, Montreal Neurological Institute; rCBF, regional cerebral blood flow; i. above, included above.

(Siemens Knoxville USA). As previously described, a total of nine scans (three conditions × three samples) were acquired. Each session consisted of 10 minutes in total. The data were reconstructed with the Ordered Subsets Expectation Maximization algorithm followed by a 4-mm Gaussian filter to a 200 × 200 × 74 matrix with zoom set equal to 2 resulting in 2.04 × 2.04 × 3–mm voxels.

Analysis of the Acquired Data

Image preprocessing was performed using PMOD (version 3.3; PMOD Technologies, Switzerland), and statistical analysis was carried out using the Statistical Parametric Mapping 8 program (Institute of Neurology, University College of London, England, U.K.) implemented in Matlab version 2011a (MathWorks Inc., Natick, MA, USA). Cluster centers were anatomically located using the MRIcron software (http://www.sph.sc.edu/comd/rorden/mricron/).

Intrascan analyses of activated cortical areas were carried out in a voxelwise manner with a flexible factorial design with scan timing (prerecovery and postrecovery) and condition as factors by contrasting the brain activities for the two active stimuli conditions with the brain activity for the null condition using a statistical threshold of $p = 0.05$, uncorrected ($k = 100$, $T = 3.30$). Interscan analyses were then performed by subtracting the areas of increased $H_2{}^{15}O$ uptake in the prerecovery scan from that of the postrecovery scan for two active stimulus conditions or vice versa with a threshold of uncorrected $p = 0.0005$ ($k = 100$, $T = 4.30$).

RESULTS

Significant Activation in Sound Stimuli Conditions During the Symptomatic Period

The patient showed activation under the speech stimulus condition relative to the resting state in the bilateral primary/secondary auditory cortices (A1/A2, BAs 41/22), bilateral middle and superior frontal gyri (BAs 8/9/10/11), right inferior parietal lobule (IPL, BA 40), right precuneus (BA 7), and anterior cingulate cortex (BA 32) (Fig. 1, upper panels; Table 1). Under the noise stimulus condition, significant activation was revealed in the right angular gyrus (BA 39), right precentral gyrus (BA 4), and bilateral cerebellum (Fig. 1, lower panels; Table 1).

Significant Activation in Sound Stimuli Conditions After Recovery

After recovery, the patient displayed significant activation under the speech stimulus condition relative to the

TABLE 2. *Areas of relative activation after recovery compared with before recovery under speech and noise stimuli (uncorrected p < 0.005, k = 100 voxels, T = 4.30)*

Region	Hemisphere	BA	Peak MNI coordinates (*x*, *y*, *z*)			Cluster size (*k*)	T value
Areas of relative activation under speech stimuli							
Superior temporal gyrus	R	41/42/22	54	−14	6	859	8.6
Inferior temporal gyrus	R	20	40	0	−50	512	6.7
Middle frontal gyrus	R	6	36	14	48	207	7.5
Inferior frontal gyrus	R	9	48	4	28	i.above	5.8
Inferior frontal gyrus	R	9	40	8	30	i.above	4.8
Cerebellar tuber	R		50	−66	−30	1297	11.6
Superior parietal lobule	L	7	−38	−60	74	432	13.6
Postcentral gyrus	L	5	−34	−54	68	i.above	10.6
	L	1	−34	−34	64	i.above	5.7
Postcentral gyrus	L	3	−42	−20	42	923	8.9
Inferior frontal gyrus	L	9	−48	4	28	i.above	7.7
Inferior parietal lobule	L	40	−40	−34	40	i.above	7.4
Areas of relative activation under noise stimuli							
Middle temporal gyrus	R	21	60	−6	−10	125	7.2
Inferior temporal gyrus	R	20	18	−26	58	183	7.9
Fusiform gyrus	R	20	54	−22	−26	247	6.4
Precentral gyrus	R	4	18	−26	58		6.6
	R	6	26	−18	62	i.above	6.1
Middle frontal gyrus	R	6	26	−6	60	i.above	5.2
Inferior parietal lobule	R	40	52	−42	42	235	6.2
Cerebellar declive	R		12	−70	−16	257	6.2
Precentral gyrus	L	6	−24	−16	60	239	9.8
Medial frontal gyrus	L	6	−2	−8	50	183	8.2
Cuneus	L	19	−12	−92	24	275	7.0
Middle occipital gyrus	L	18	−26	−96	10	i.above	5.9
Inferior parietal lobule	L	40	−36	−32	44	497	7.0
Postcentral gyrus	L	3	−44	−22	42	i.above	6.7
Medial frontal gyrus	L	8	−12	28	44	129	6.8
Precuneus	L	7	−12	−44	56	106	6.4
Postcentral gyrus	L	4	−12	−32	60	i.above	5.1
Inferior parietal lobule	L	40	−40	−54	40	140	5.4
Superior parietal lobule	L	7	−38	−64	50	i.above	5.4
Supramarginal gyrus	L	40	−54	−52	30	i.above	5.1
Cerebellar uvula	L		−34	−72	−24	491	10.4
Cerebellar inferior semiluar lobule	L		−28	−64	−44	680	8.8

BA indicates Brodmann area; MNI, Montreal Neurological Institute; rCBF, regional cerebral blood flow; i. above, included above.

resting state in the bilateral A1/A2 (Fig. 2, upper panels; Table 1). Under the noise stimulus condition, significant activation was observed in the bilateral IPL (BA 40), right middle occipital gyrus (BA 19), right insula (BA 13), right cerebellar declive, and left supramarginal gyrus (BA 40) (Fig. 2, lower panels; Table 1).

Comparison Between Prerecovery and Postrecovery

Under the speech stimulus condition, greater activation in the postrecovery state relative to the prerecovery state was observed in the right A1/A2 (BAs 41/42/22), right inferior temporal gyrus (BA 20), right middle frontal gyrus (BA 6), right inferior frontal gyrus (BA 9), left inferior frontal gyrus (BA 9), left superior parietal lobule (BA 7), and left IPL (BA 40) (Fig. 3, upper panels; Table 2). Also, compared with the prerecovery state, the postrecovery state revealed relative activation in the ventral and dorsal parietal cortices (VPC/DPC).

DISCUSSION

The patient's history and clinical course exactly corresponded to conversion deafness. Also, electrophysiologic tests revealed no device-related abnormal findings. Thus, we performed $H_2{}^{15}O$-PET scan to confirm the intact ascending auditory pathway. By observing the activation of the A1/A2 by speech and nonspeech stimuli, we confirmed that the integrity of the ascending auditory pathway was intact. In other words, the patient was not able to perceive sound stimuli albeit he was receiving sound stimuli up to the cortical level.

The comparison between prerecovery and postrecovery images revealed significant areas of relative activation that may be responsible for the differences in the level of auditory perception (Fig. 3). Compared with the prerecovery state, the postrecovery state showed relative activation in the right A1/A2. In addition, the postrecovery scans revealed stark activation in the prefrontal/parietal areas relative to the prerecovery scans. Previous literature contrasting between conscious and nonconscious processing have indicated objective neural measures of conscious access to sensory stimulus as a late amplification of relevant sensory activity and ''ignition'' of a large-scale prefronto-parietal network (9,10). In this regard, the relative activation of the prefrontal, parietal, and temporal area

in the current case may explain the restoration of conscious auditory perception.

The relative activations of the VPC/DPC suggest another possible mechanism. When a relevant stimulus is presented, the VPC is suggested to send a bottom-up *circuit breaker* signal to the DPC (11), which shifts attention to the previously unattended stimulus by a top-down attentional modulation (12). From this point of view, the current case may have adopted auditory stimuli as relevant by activating the VPC, and the DPC shifted attention to perceive auditory stimuli. In other words, relative deactivation of the VPC and DPC during the symptomatic period may designate failures of circuit breaking and attentional shift.

Several brain regions have been suggested to be involved in the pathogenesis of various conversion disorders. A recent systematic review concluded that the sample sizes in the neuroimaging studies of conversion disorder have been too small that it remains unclear which findings represent signal or noise (1). Our findings are also limited by the same issue. Although this is the first molecular imaging study on conversion deafness, it is an assumption and interpretation of a single case of conversion deafness and indirect regional cerebral blood flow measurement with $H_2{}^{15}O$-PET. Future studies in a large group of patients with other imaging modalities such as quantitative electroencephalography (13–15) or PET (16) are still mandatory.

As in the current study, $H_2{}^{15}O$-PET may be of help in verifying the integrity of the ascending auditory pathway up to the cortical level in cases of CI users with conversion deafness. Stimulation of the central auditory pathway can be easily evaluated using electrically evoked auditory brainstem response (EABR) or cortical auditory evoked potentials (CAEPs). EABR or CAEPs are advantageous over PET scans because EABR or CAEP can be easily performed with less cost. Nonetheless, PET scans may be of additional value because they visualize cortical activities other than auditory cortex, and thus, we may be able to understand the pathophysiology of conversion deafness.

CONCLUSION

Taken together, the current study suggests molecular imaging methods as an adjunct diagnostic approach for a CI patient with possible conversion deafness. Relative deactivation of the prefronto-parieto-temporal network or dysfunction in the VPC-DPC–based attention shifting system may be responsible for conversion deafness.

Acknowledgments: The authors thank Jan Ost, Bram Van Achteren, Bjorn Devree, and Pieter van Looy for help in preparing this manuscript. Also, the first author thanks Dr. D. Y. Yoon for giving precious support to the study.

REFERENCES

1. Browning M, Fletcher P, Sharpe M. Can neuroimaging help us to understand and classify somatoform disorders? A systematic and critical review. *Psychosom Med* 2011;73:173–84.
2. Pracy JP, Walsh RM, Mepham GA, et al. Childhood pseudohypacusis. *Int J Pediatr Otorhinolaryngol* 1996;37:143–9.
3. Carlson ML, Archibald DJ, Gifford RH, et al. Conversion disorder: a missed diagnosis leading to cochlear reimplantation. *Otol Neurotol* 2011;32:36–8.
4. Battmer RD, Backous DD, Balkany TJ, et al. International classification of reliability for implanted cochlear implant receiver stimulators. *Otol Neurotol* 2010;31:1190–3.
5. Song JJ, Yoo YT, An YH, et al. Comorbid benign paroxysmal positional vertigo in idiopathic sudden sensorineural hearing loss: an ominous sign for hearing recovery. *Otol Neurotol* 2012;33:137–41.
6. Chang MY, Song JJ, Kim JS, et al. Contralateral suppression of distortion-product otoacoustic emissions: a potential diagnostic tool to evaluate the vestibular nerve. *Med Hypotheses* 2013;81:830–3.
7. Stone J, LaFrance WC Jr, Levenson JL, et al. Issues for *DSM-5*: conversion disorder. *Am J Psychiatry* 2010;167:626–7.
8. Song JJ, Vanneste S, Van de Heyning P, et al. Transcranial direct current stimulation in tinnitus patients: a systemic review and meta-analysis. *ScientificWorldJournal* 2012;2012:427941.
9. Sadaghiani S, Hesselmann G, Kleinschmidt A. Distributed and antagonistic contributions of ongoing activity fluctuations to auditory stimulus detection. *J Neurosci* 2009;29:13410–7.
10. Dehaene S, Changeux JP. Experimental and theoretical approaches to conscious processing. *Neuron* 2011;70:200–27.
11. Cabeza R, Ciaramelli E, Olson IR, et al. The parietal cortex and episodic memory: an attentional account. *Nat Rev Neurosci* 2008;9:613–25.
12. Song JJ, De Ridder D, Van de Heyning P, et al. Mapping tinnitus-related brain activation: an activation-likelihood estimation metaanalysis of PET studies. *J Nucl Med* 2012;53:1550–7.
13. Song JJ, Vanneste S, Schlee W, et al. Onset-related differences in neural substrates of tinnitus-related distress: the anterior cingulate cortex in late-onset tinnitus, and the frontal cortex in early-onset tinnitus. *Brain Struct Funct* 2013 Oct 18 [Epub ahead of print].
14. Song JJ, Punte AK, De Ridder D, et al. Neural substrates predicting improvement of tinnitus after cochlear implantation in patients with single-sided deafness. *Hear Res* 2013;299:1–9.
15. Song JJ, De Ridder D, Weisz N, et al. Hyperacusis-associated pathological resting-state brain oscillations in the tinnitus brain: a hyperresponsiveness network with paradoxically inactive auditory cortex. *Brain Struct Funct* 2014;219:1113–28.
16. Song JJ, Lee HJ, Kang H, et al. Effects of congruent and incongruent visual cues on speech perception and brain activity in cochlear implant users. *Brain Struct Funct* 2014 Jan 9 [Epub ahead of print].